Ceramics International 45 (2019) 2060–2068

Contents lists available at ScienceDirect

Ceramics International

journal homepage: www.elsevier.com/locate/ceramint

Enhanced thermoelectric performance of Cu_2ZnSnS_4 (CZTS) by incorporating Ag nanoparticles

Sarita Devi Sharma[a], B. Khasimsaheb[a,b], Y.Y. Chen[b], S. Neeleshwar[a,*]

[a] University School of Basic & Applied Science, GGS Indraprastha University, Delhi 110078, India
[b] Institute of Physics, Academia Sinica, Taipei 11529, Taiwan, ROC

ARTICLE INFO

Keywords:
CZTS
Hot pressing
Electrical conductivity
Power factor
Figure of merit

ABSTRACT

Thermoelectric properties of Cu_2ZnSnS_4 (CZTS) microspheres on addition of Ag nanoparticles in different weight percentage (0, 0.5%, and 1%) were investigated in the temperature range from 300 K to 623 K. CZTS/Ag thermoelectric composites were fabricated by mixing the CZTS powder synthesized by microwave method and silver nanoparticles (Ag NPs) followed by hot pressing at 623 K. Due to the addition of highly conductive Ag NPs in the composites, the electrical conductivity increased systematically from parent sample value of 852 Sm^{-1} to the values of CZTS/0.5 wt% and CZTS/1 wt% composites which were 4291 Sm^{-1} and 6369 Sm^{-1} respectively at room temperature while maintaining moderate Seebeck coefficient. Improved power factor values (117 $\mu W/mK^2$ and 84.6 $\mu W/mK^2$) for the CZTS/ (0.5, 1 wt%) Ag composites compared to bare sample (55 $\mu W/mK^2$) were observed at 623 K. Besides, a lower thermal conductivity (~0.42 W/m K) for CZTS/0.5 wt% Ag composite in comparison to the bare sample (~0.49 W/m K) at 623 K was also obtained due to phonon scattering by dispersed Ag NPs. It was observed that CZTS/0.5 wt% Ag sample exhibited a figure of merit 0.17 at 623 K almost 2.5 times more than parent CZTS sample (0.069), which was attributed to the improvement in the electrical conductivity and reduction in the total thermal conductivity. These results demonstrate that addition of Ag NPs into the CZTS host material has a potential to enhance the thermoelectric performance.

1. Introduction

Increasing energy usage in the worldwide has forced the researchers to develop various renewable energy technologies. Thermoelectric technology is a type of renewable energy technology based on Seebeck effect which can tap the waste heat from surrounding and converts it to the useful electrical energy [1,2]. Energy conversion efficiency of the thermoelectric materials is represented by a dimensionless quantity named as figure of merit, $ZT = \sigma S^2 T/\kappa$, where σ is electrical conductivity, S is Seebeck coefficient, κ is thermal conductivity and T is temperature. Due to the interrelated properties of all these parameters one has to compromise in order to obtain decent value of ZT [3]. Some of the previously reported highly efficient thermoelectric compositions for power generation applications include half-Heuslers [4,5], silicides [6], lead telluride [7] and bismuth telluride [8]. Most of the conventional thermoelectric materials like Bi_2Te_3, PbTe, Si-Ge and $CoSb_3$ consist of rare earth, expensive or environmental hazardous elements (e, g Pb, Te, Ge, Sb etc.) thus hindering their practical usage on large scale [6]. Scientific community is constantly exploring a wide range of cost effective and eco friendly thermoelectric materials which can be synthesized in bulk form. One such type of thermoelectric materials are copper based chalcogenides (S and Se) i,e binary superionic conductors (Cu_2Se, Cu_2S), ternary (Cu_2SnSe_3, Cu_2SnS_3 etc.) and quarternary semiconductors ($Cu_2ZnSnSe_4$,Cu_2ZnSnS_4) which consist of non-toxic, eco- friendly and abundant elements in earth crust [9,10]. In recent years, close attention has been paid on the investigation of thermoelectric properties of typically wide band gap copper zinc tin sulphur/selenide (CZTS/Se) materials due to their complex structure [11,12]. Owing to their complex structure, the thermal conductivity of copper quaternary chalcogenides are much less compared to many other conventional thermoelectric materials and their large band gap can reduce the bipolar effect which is generally present in narrow band gap thermoelectric materials [13].

Cu_2ZnSnS_4 (CZTS) is a thermoelectric material which possesses a low thermal conductivity, high Seebeck coefficient values but a low value of electrical conductivity [14,15]. The thermoelectric properties of CZTS synthesized by different synthesis techniques like solid state reaction, hot injection, colloidal, hydrothermal and flow reactor method via Cu or Ni doping at the Zn sites in the bulk or nanocrystals materials and doping S sites via Se had been explored in literature

* Corresponding author.
E-mail address: sn@ipu.ac.in (S. Neeleshwar).

https://doi.org/10.1016/j.ceramint.2018.10.109
Received 30 August 2018; Received in revised form 5 October 2018; Accepted 13 October 2018
Available online 16 October 2018

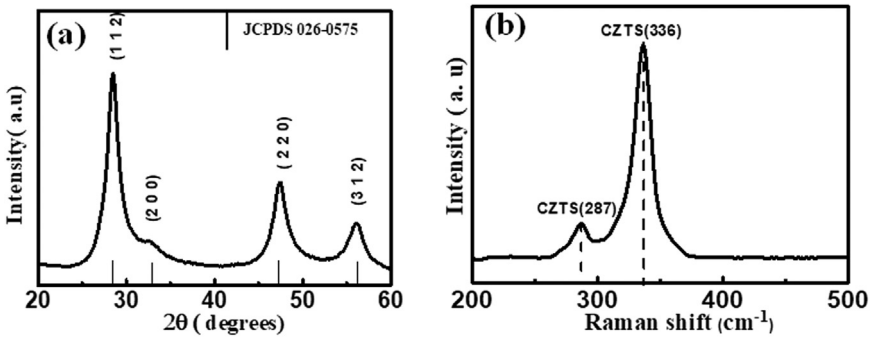

Fig. 1. (a) XRD pattern, and (b) Raman spectrum of CZTS particles.

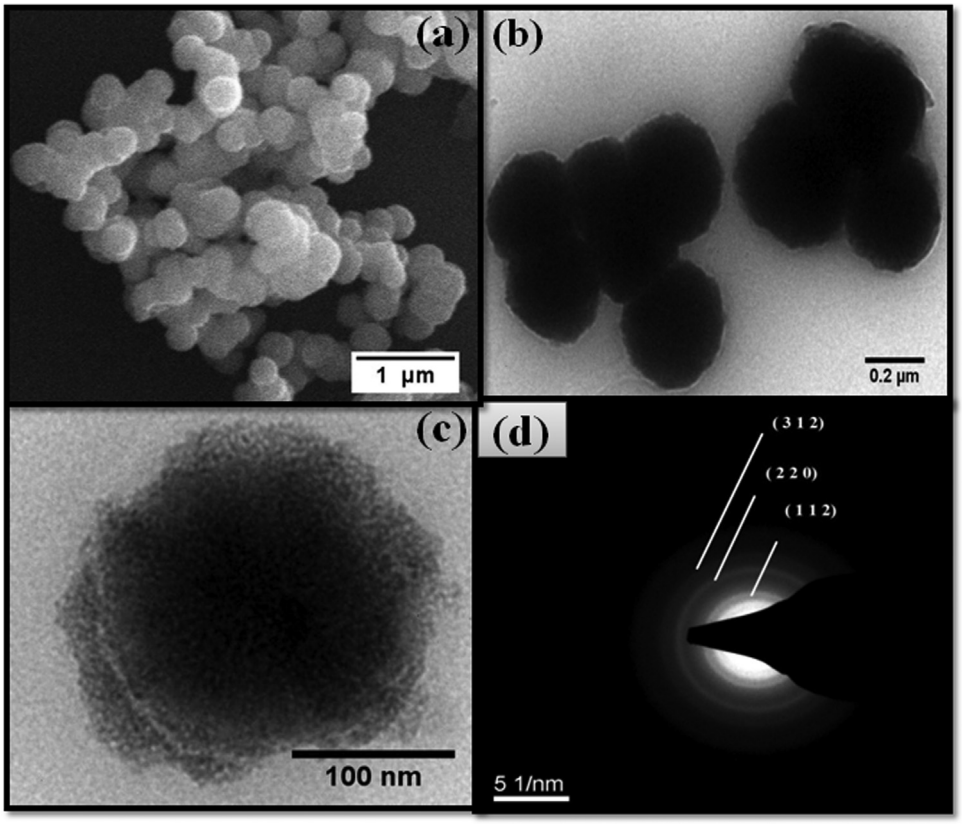

Fig. 2. (a) SEM image, (b) low, (c) high magnification TEM images, and (d) SAED pattern of as prepared CZTS particles.

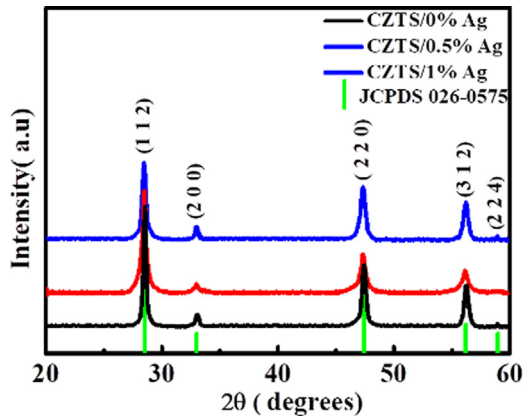

Fig. 3. XRD patterns of CZTS/x (x = 0, 0.5, and 1) wt% Ag hot pressed composites with standard JCPDS data.

[14–18]. In comparison, the preparation of low-dimensional nanocomposites had not yet been investigated and may be beneficial for the enhancement of thermoelectric properties of CZTS system. There are various strategies to enhance the thermoelectric performance of materials either by maximizing power factor or by fabricating nanocomposites [19,20]. Many efforts have been made to improve ZT by introducing a low-dimensional nanophase into thermoelectric matrix by fabricating the nanocomposites of semiconductor host with the metallic particle nanoinclusions [21,22]. It has been reported that addition of metal nanoparticles like Ag, Cu in different % to the thermoelectric materials e.g Bi_2Te_3 (0–5 vol% Ag), $Ca_3Co_4O_9$ (0–2.5 vol% Ag), $Bi_{0.5}Sb_{1.5}Te_3$ (0–0.2 wt% Ag, 0–0.2 wt% Cu), PbS (0–4.7 mol% Ag), $Ba_{0.3}Co_4Sb_{12}$ (0.5 wt% Ag), In_4Se_3(0–0.5 wt% Cu) is advantageous in enhancing the electrical conductivity [23–28]. These metal particles with high electrical conductivities present at grain boundaries can act as electrical connectors between the different grains [27,29]. Also, finely dispersed metal nano particles in Bi_2Te_3 and $Ba_{0.3}Co_4Sb_{12}$ for optimum quantity lead to suppression of lattice thermal conductivity due to the scattering of phonons at increased grain boundaries [23,27].

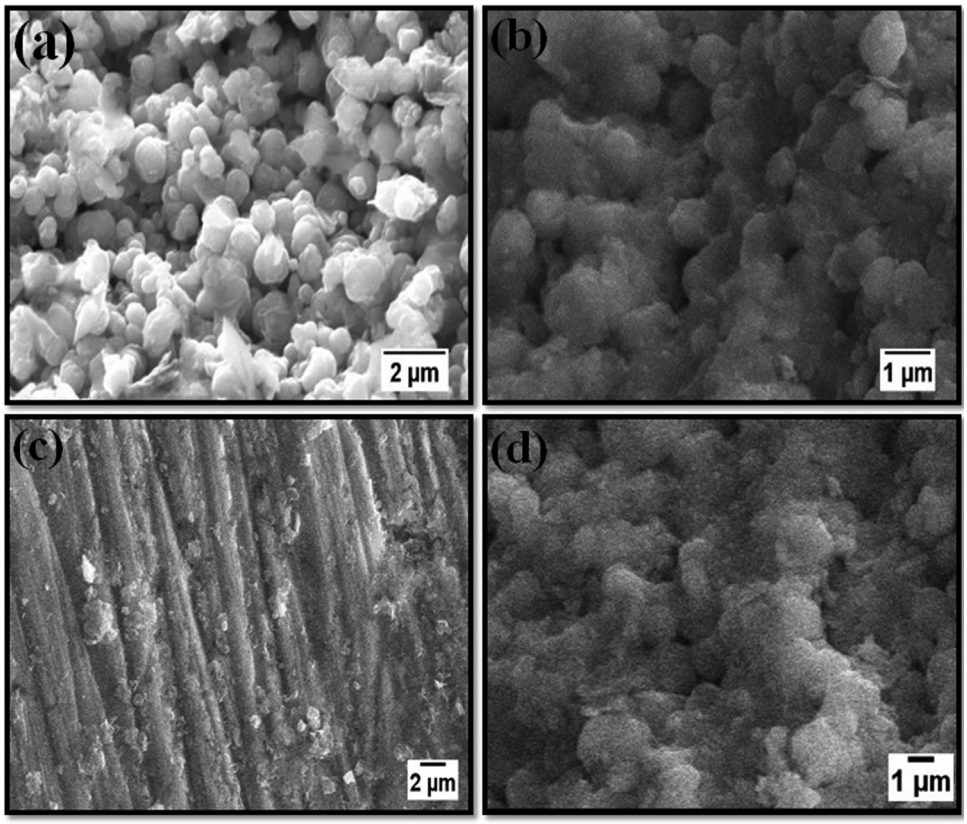

Fig. 4. SEM micrographs of (a) hot pressed bare CZTS sample, (b) and (c) fractured surfaces of CZTS/0.5 wt% Ag composite consisting number of nanoparticles, and (d) CZTS/1 wt% Ag composite.

Gao et al. [30] showed for CdO: Ag (0.5–3 at%) nanocomposite that enhanced carrier filtering effect increases the Seebeck coefficient. Liu et al. [31] summarized almost all such literature of metallic inclusions into different thermoelectric materials. Therefore, simultaneous increment in power factor and reduction in thermal conductivity is also possible for the CZTS system by appropriate inclusion of Ag NPs.

Based on above considerations, an approach to enhance the thermoelectric properties of CZTS material with addition of Ag NPs is followed in the present study. As per literature survey, this might be the first attempt in CZTS system for investigation of thermoelectric properties by incorporation of metal nanoparticles. Achieving a pure CZTS phase in bulk quantity by any fabrication techniques is itself a big challenge as either formation of some secondary phases are often observed along with CZTS phase or complex reactions for number of hours are required [17,32]. Through this report, two major issues of CZTS are addressed (a) synthesis of pure single CZTS phase via microwave method which is versatile, less time consuming, and involves rapid nucleation process [33] and (b) electrical conductivity improvement with incorporation of highly conductive Ag NPs. CZTS particles were mixed with different wt% of Ag particles followed by hot pressing and enhanced thermoelectric performance was obtained for composite systems as compared to the parent CZTS.

2. Experimental section

2.1. Synthesis of CZTS particles

CZTS particles were synthesized by microwave method similar to reported in our earlier work [34]. 2 mmol of copper chloride dihydrate ($CuCl_2{\cdot}2H_2O$; 99%, Alfa Aeser) was added to 70 ml of ethylene glycol (SRL chemicals) solution in round bound flask placed on magnetic stirrer. After the complete mixing of copper precursor, 1 mmol of zinc chloride anhydrous ($ZnCl_2$; 98%, Alfa Aeser) was added to reaction mixture followed by addition of 1 mmol of tin chloride dihydrate ($SnCl_2{\cdot}2H_2O$; 99% Alfa Aeser). Then, 5 mmol of thiourea (NH_2CSNH_2; 99%, SRL chemicals) was added to reaction mixture and was stirred till a transparent solution was obtained. The solution flask was kept in microwave oven 800 W output power (2.45 MHz) at a temperature of 170 °C for almost 8–10 min and after that black coloured precipitates were obtained. This black product was washed with ethanol and distilled water for several times to remove present any by-products or impurity. The precipitates were dried in the oven at a temperature of 50 °C for 10 h. The commercially procured Ag NPs (20–40 nm) in different wt% (0, 0.5 and 1) were added to the CZTS powder in order to prepare CZTS composites. Mixture of powders were ground in mortar pestle, and then were hot pressed using 20 mm graphite die at a temperature of 623 K and a pressure of 80 MPa in vacuum for 15 min.

2.2. Characterizations

The crystal structure and phase of the prepared CZTS particles as well as composite systems were studied by X-Ray diffraction (XRD, PAN Analytical) using Cu Kα radiation. The Raman spectrum for the CZTS particles was obtained by Micro Raman spectroscopy (HORIBA Scientific with a laser wavelength of 514 nm). Microstructures were examined by a field emission scanning electron microscope (FESEM, FEI NOVA) equipped with energy-dispersive X-ray spectroscopy (EDS) system and transmission electron spectroscopy (TEM, JEOL, JEM-2100plus). Chemical states of all the elements including Ag in the composite system were examined by using X-ray photoelectron spectroscopy (XPS, Omicron Nano Technology). The thermoelectric properties of the composite materials were investigated in the temperature range of 300 K to 623 K. The electrical conductivity and Seebeck coefficient of bar shaped samples were measured simultaneously by using a

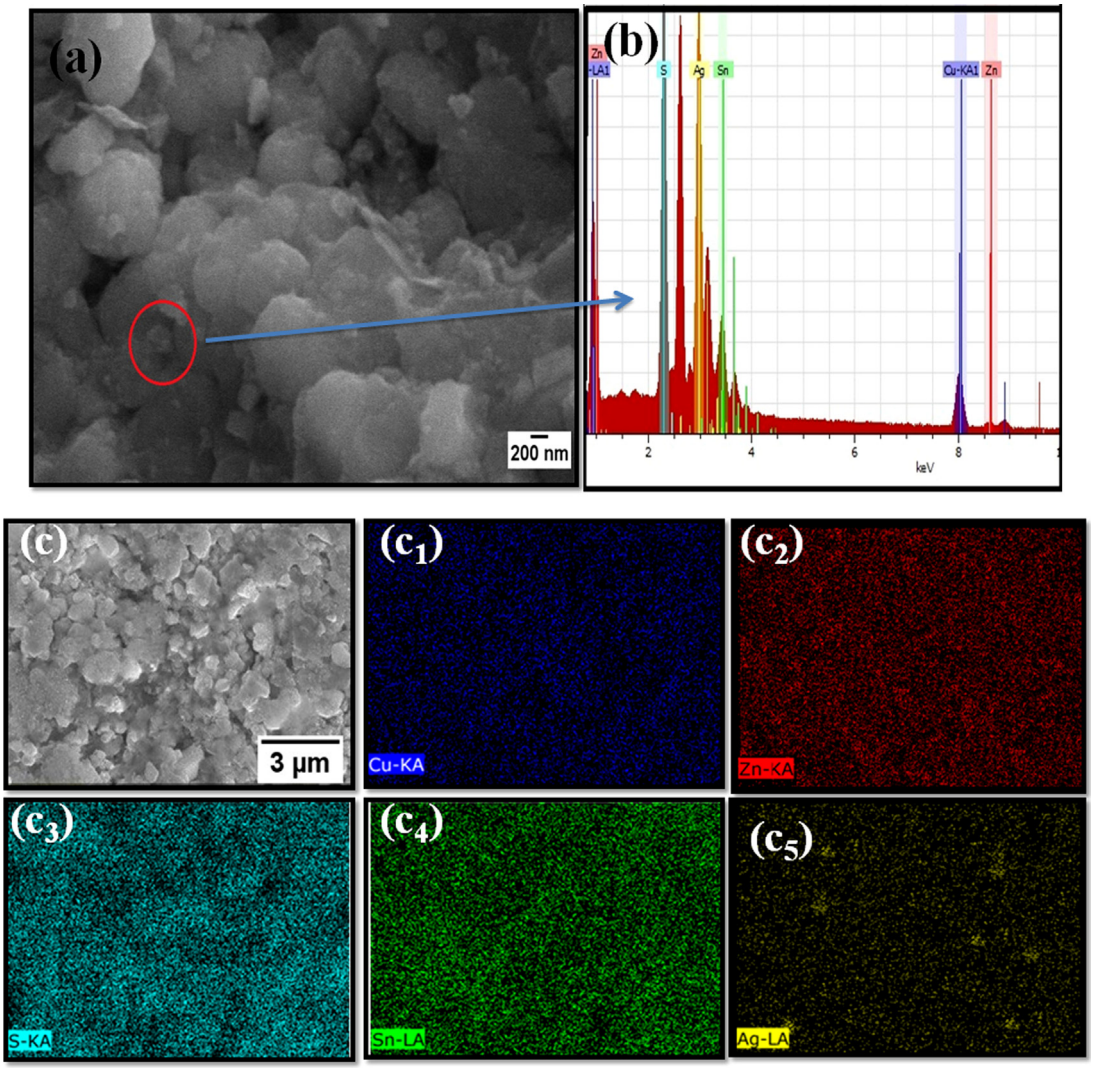

Fig. 5. (a) High resolution SEM image, (b) EDS pattern with Ag peak, and (c) Elemental mapping showing presence of all elements in uniform distribution along with silver particles for CZTS/0.5 wt% Ag composite.

commercial four-probe apparatus (ULVAC- ZEM-3). Carrier concentration and mobility of all the composite samples at room temperature were extracted from Hall Effect measurements through the Vander Pauw method. The thermal diffusivity, λ measurements were performed on all the samples with round shape disks by the laser flash method (LFA 1000 laser flash). The specific heat, Cp was measured on a DSC-Q2000 instrument (TA). Sample density ρ was calculated by Archimedes' method and densities of the samples with 0%, 0.5% and 1% Ag NPs were 4.19 g/cm^3, 4.33 g/cm^{3,} 4.42 g/cm^3 respectively. Uncertainty in the measurement of transport measurements were: ± 6% for thermal diffusivity, ± 5% for electrical conductivity, ± 7% for Seebeck coefficient, ± 5% for specific heat and ± 0.5% for density.

3. Results and discussions

3.1. Structural and morphological characterizations

Fig. 1. (a) represents the XRD pattern of as synthesized CZTS powder sample. The four diffraction peaks at 28.52°, 32.9°, 47.5° and 56.41° are attributed to (112), (200), (220) and (312) planes of CZTS with tetragonal crystal structure well matching with the JCPDS card no. 26–0575 [15,17]. Average crystallite size calculated for the major peaks (112) and (220) using Scherrer formula is 10.95 nm. Some binary and ternary compounds i, e ZnS, Cu_2SnS_3 possess the diffraction pattern similar to CZTS [17]. So, individually XRD result cannot claim the presence of only CZTS tetragonal phase. Hence, Raman spectroscopy was further employed to determine the phase purity and structure of CZTS particles. Raman spectrum for the CZTS powder sample in the range 200–500 cm^{-1} is shown in Fig. 1(b). The existence of a shoulder peak at 287 cm^{-1} and an intense peak at 336.7 cm^{-1} are due to the vibration of the S atoms in CZTS lattice. Absence of any other peaks corresponding to binary or ternary compounds confirms the presence of only pure CZTS phase in the material [16,35]. The result of Raman spectrum is consistent with the XRD pattern of as synthesized CZTS powder. Morphology of the synthesized CZTS particles was analysed by scanning electron microscopy (SEM) and transmission electron microscopy (TEM). Fig. 2. (a) shows the SEM image for CZTS particles with sphere like morphology which are connected to adjacent ones. To further confirm structure and uniform morphology, TEM images are presented in Fig. 2. (b) and (c). Uniform sphere like shape for particles with size ranging from 300 to 350 nm is observed for as synthesized CZTS sample. As shown in Fig. 2. (c), these spherical particles are consisting of number of nanoparticles. SAED pattern confirms the polycrystalline structure and different planes of synthesized CZTS particles well matching with the XRD results as shown in Fig. 2. (d). Hence combined XRD, RAMAN spectroscopy and TEM data affirms the formation of single pure tetragonal phase CZTS microspheres by the microwave synthesis.

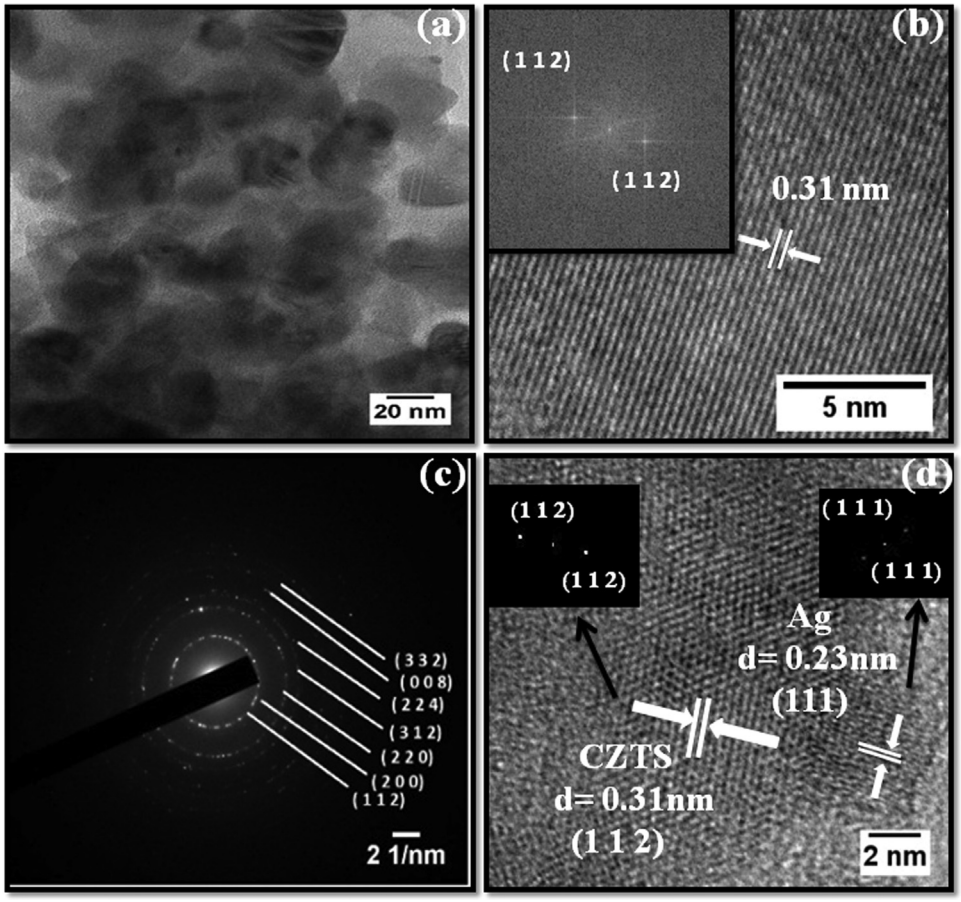

Fig. 6. (a) TEM image of CZTS/0.5 wt% Ag composite system containing nanoparticles, (b) HRTEM image of CZTS particles (inset FFT image corresponding to (112) plane), (c) SAED pattern showing polycrystalline nature of CZTS, and (d) HRTEM image of CZTS/0.5 wt% Ag composite corresponding to CZTS and Ag planes (inset FFT images for CZTS (1 1 2) plane and Ag (1 1 1) plane).

All the hot pressed CZTS/(0, 0.5, 1) wt% Ag composites were characterized by X-ray diffraction. Fig. 3. represents (XRD) patterns of the Cu_2ZnSnS_4/ x wt% Ag (x = 0, 0.5, 1) composites, which are indexable to the kesterite-type Cu_2ZnSnS_4 with space group I4 (PDF#26–0565) [15]. It was observed that there is no new phase formation or phase change occurs after hot pressing (HP) of all the samples. No peak of metallic Ag is detected in the XRD patterns of composites CZTS/x (x = 0.5, 1) wt% Ag due to the less weight fractions of Ag. Moreover, there is no traceable shift of the diffraction peak angles, indicating that most of Ag exists at the grain boundaries or interstitial sites as metal form.

Morphological analysis of all the hot pressed samples without and with Ag NPs was carried out and almost similar microstructures with enlargement of grains were observed for all the samples. Fig. 4. (a) represents the SEM micrograph of the bare sample which is consisting of linked sphere like particles with increased grain size (~800 nm) due to the hot pressing of powder sample. SEM images for fractured surfaces of CZTS/0.5 wt% Ag and CZTS/1 wt% Ag composite samples are shown in Fig. 4. (b), (c) and (d). Few small nanoparticles along with the bigger grains are present in these SEM micrographs which may correspond to Ag NPs as these nanoparticles were not present in parent hot pressed CZTS sample. As depicted in SEM images of Fig. 4, the grains for all specimens are closely packed which is in consistence with higher density of composites. To further confirm the presence and distribution of Ag NPs in the composite, EDS analysis and the elemental mapping along with FE-SEM image of hot pressed CZTS/0.5 wt% Ag sample are shown in Fig. 5. Some nanoparticles with sizes of few nanometres are observed at the grain boundary and on surface of grains as shown in SEM micrograph of Fig. 5. (a). The EDS analysis for the circled part in Fig. 5. (b) clearly confirms the existence of Ag NPs and presence of all other elements of CZTS compound. Elemental mapping reveals the existence and uniform distribution of Ag NPs in CZTS/0.5 wt% Ag composite as presented in Fig. 5. (c). According to this analysis, Ag NPs are present either on the surface of grains or in between grain boundaries of CZTS/0.5 wt% Ag composite. Fig. 6. (a) shows the TEM image of CZTS/0.5 wt% Ag composite sample with number of nanoparticles (35–45 nm) embedded in composite. High-resolution TEM (HRTEM) image in Fig. 6(b) for a single CZTS nanoparticle shows a well-resolved lattice pattern, indicates its crystalline nature. Inset of Fig. 6. (b) represents FFT obtained from the HRTEM image which corresponds to the (112) lattice plane of CZTS. However, the selected area electron diffraction (SAED) pattern as shown in Fig. 6. (c) clearly indicates the poly crystalline nature of the CZTS. HRTEM image in Fig. 6. (d) represents the d-spacing of 0.31 nm which corresponds to (1 1 2) plane of CZTS as well as d value of 0.23 nm for (1 1 1) plane of Ag according to the standard XRD data [23]. Thus, the TEM analysis also confirms the presence of Ag in the polycrystalline CZTS system.

To verify that the dispersed Ag NPs in the CZTS system exist in metallic form, XPS study was also carried out on the CZTS/0.5 wt% Ag sample as presented in Fig. 7. Oxidation state of other constituent elements in CZTS was also verified by XPS analysis. As shown in Fig. 7. (a), the XPS spectrum peaks of Ag $3d_{5/2}$ and Ag $3d_{3/2}$ are located at binding energies 367.95 and 373.97 eV, respectively. This verifies the 0 oxidation state for Ag NPs which is suggesting that metallic Ag inclusions exist in the CZTS matrix [29,30]. Peak differences of XPS spectra from Fig. 7. (b), (c), (d) and (e) confirms the Cu^{+}, Zn^{2+}, Sn^{+4} and S^{2-} states for other constituent elements of CZTS well resemblance with reported values [35–37]. Although not detected by XRD, SEM, HRTEM and XPS observations clearly confirm the presence of Ag NPs in metallic form distributed in polycrystalline CZTS/0.5 wt% Ag composite.

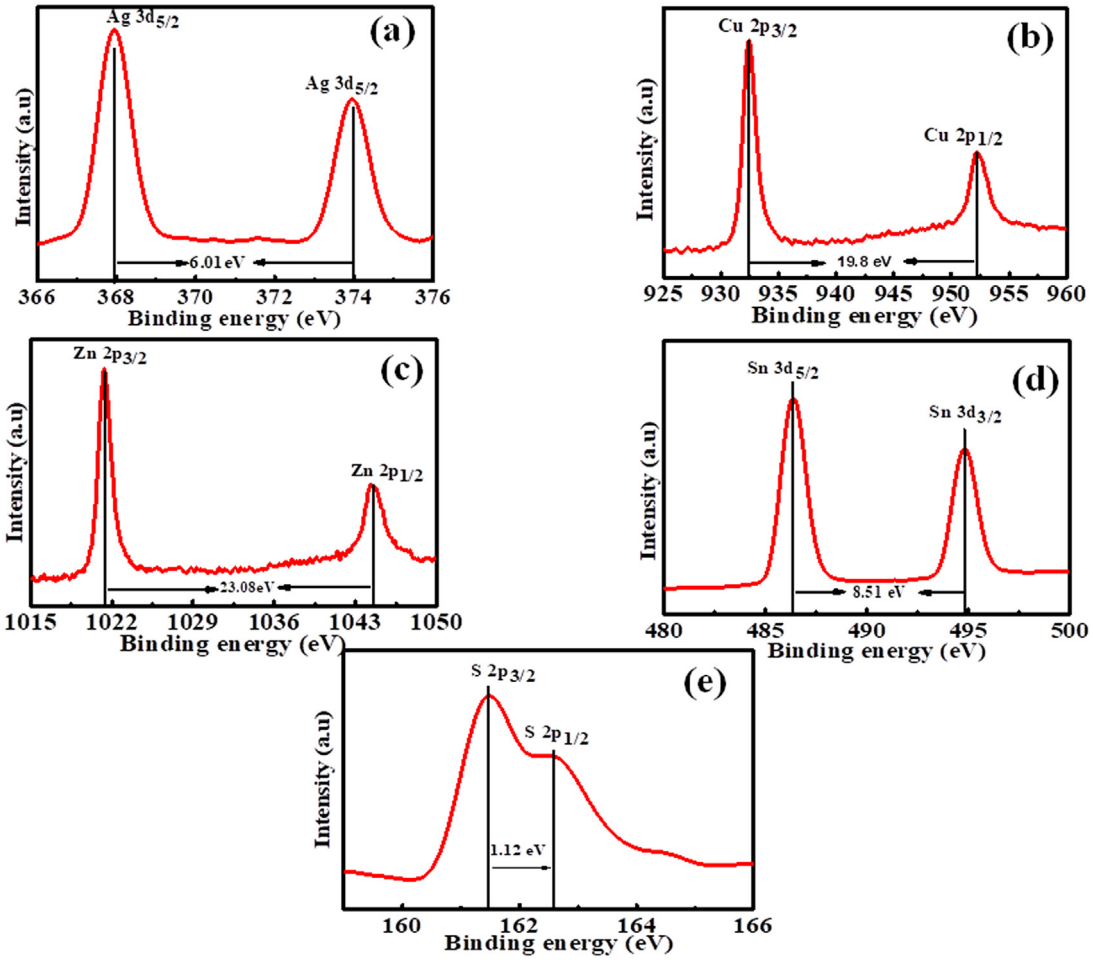

Fig. 7. XPS of hot pressed CZTS/0.5 wt% Ag composite (a) spectrum shows presence of Ag in metallic form, spectra for (b) Cu 2p, (c) Zn 2p, (d) Sn 3d, and (e) S 2p respectively.

3.2. Thermoelectric characterizations

3.2.1. Electric transport properties

The electric transport properties for CZTS/xwt% Ag (x = 0%, 0.5%, 1%) composites were investigated as shown in Fig. 8. The temperature dependence of electrical conductivity (σ) for all samples from 300–623 K is shown in Fig. 8. (a). The electrical conductivity of all the samples increases with increase of temperature, showing the semiconductor like behaviour. Electrical conductivity for parent CZTS sample is 852.49 S/m at room temperature which is nearly similar to the electrical conductivity of Cu-rich CZTS nanocrystals [15]. For CZTS/0.5 wt% Ag, σ increases to a value of 4291.84 S/m and this value is further increased to value 6369.3 S/m for CZTS/1 wt% Ag composite at room temperature. Sample with 1 wt% silver has the highest concentration of Ag in this study, possessing the highest electrical conductivity with a maximum value of 12151 S/m at 540 K. Incorporation of noble metal like Ag in thermoelectric materials usually enhances the transport properties. Addition of Ag to composites can increase the carrier concentrations or for lesser amount of Ag NPs with size smaller than matrix grains, Ag particles are usually present within the matrix [23,26]. Few of the Ag NPs can be diffused in the matrix during sintering or are present in the interstitial sites [25,27]. The inset in Fig. 8(a) gives the carrier concentration and mobility for all the samples at room temperature as determined by Hall measurements. Carrier concentration (n) is found to be increasing from 3.15×10^{19} cm $^{-3}$ for the bare CZTS sample to 4.9×10^{19} cm $^{-3}$ for CZTS/ 0.5 wt% Ag composite and to 5.1×10^{19} cm $^{-3}$ for CZTS/1 wt% Ag composite whereas mobility (μ) rises from 2.7 $cm^2V^{-1}s^{-1}$ for bare CZTS to 5.47 $cm^2V^{-1}s^{-1}$ for CZTS/0.5 wt% Ag composite and to 7.79 $cm^2V^{-1}s^{-1}$ for CZTS/1 wt% Ag composite. Same behaviour of carrier concentration and mobility was also observed for Ag incorporated PbS or SiGe thermoelectric materials [26,38]. In the present study of CZTS composites as indicated by morphological analysis, the dispersed metallic Ag particles with high conductivity may be acting as electrical bridge between the grains, which lead to the easy flow of carriers at grain boundary and thus the conductivity of the composites increases [24,39]. Also, the electrical conductivity (σ) depends on the carrier concentration (n) and mobility of charge carriers (μ) as given by relation, $\sigma = ne\mu$ [39]. Hence remarkable increase in electrical conductivity observed for CZTS/ Ag composites is probably due to increased carrier concentration and electrical bridging between grains on addition of highly conductive Ag NPs. The value of electrical conductivity for Ag added composites is even higher or comparable to that reported for the Cu or Ni doped CZTS systems [15,16] as compared in Table 1. Small decrease in electrical conductivity at higher temperature for all samples may be due to the scattering of charge carriers with decrease in mobility.

Fig. 8. (b) represents the temperature variation of Seebeck coefficient (*S*) for composite samples CZTS/xwt% Ag (x = 0, 0.5, 1). Seebeck coefficient follows a trend similar to that for the reported CZTS systems [14,15]. Positive values of Seebeck coefficient (S) confirm the p-type semiconductor behaviour for these composites. For pure CZTS sample, Seebeck coefficient value at room temperature is 139 μV/K and reaches a value 228 μV/K at 623 K which is almost in the range for Seebeck coefficient values for CZTS in previous reports as given in Table 1 [15,16]. Seebeck coefficient value decreases with the addition of 0.5 wt

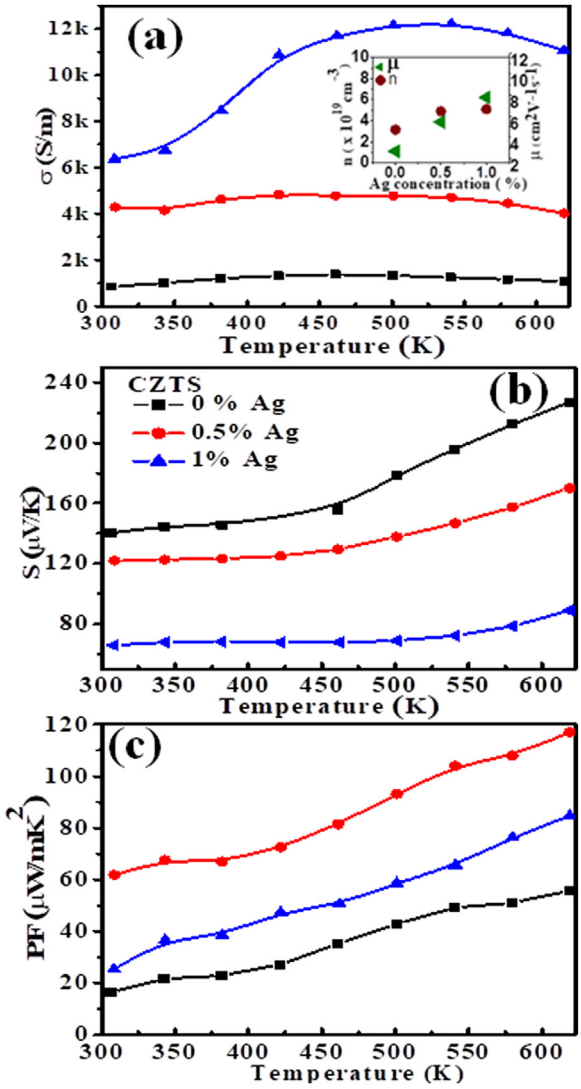

Fig. 8. Temperature dependence of (a) electrical conductivity (inset carrier concentration and mobility values for composites at room temperature), (b) Seebeck coefficient, and (c) Power factor of CZTS/x wt% Ag (x = 0, 0.5, 1) composite samples.

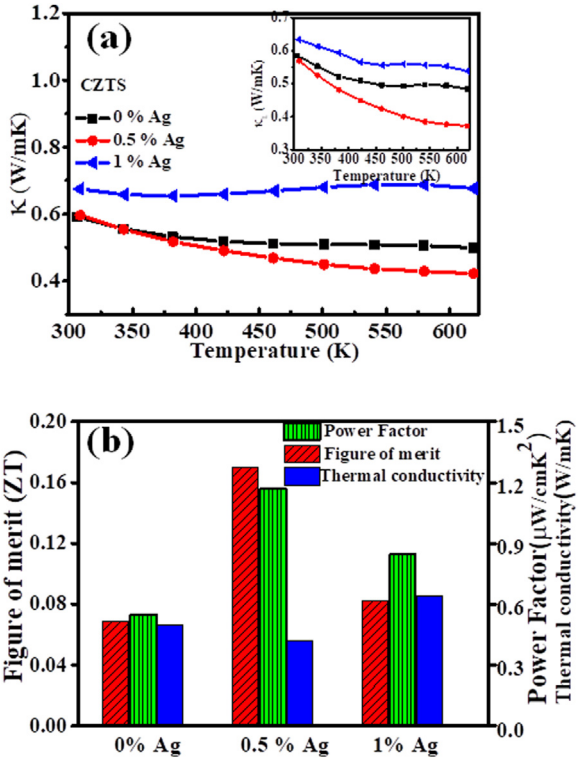

Fig. 9. (a) Temperature dependence of thermal conductivity of CZTS/xwt% Ag (x = 0, 0.5, and 1) samples, and (b) bar diagram of power factor (P), thermal conductivity (κ) and figure of merit (ZT) for all samples at 623 K.

% and 1 wt% Ag NPs to the CZTS matrix. Such differences in the behaviour of Seebeck coefficient of these samples are consistent with the electrical conductivity results. The Seebeck coefficient value for CZTS/0.5 wt% Ag composite at room temperature is 120 μV/K and reaches its highest value 171 μV/K at 623 K. But S deceases sharply for the CZTS/1 wt% Ag composite with a value 65 μV/K at room temperature and a maximum value 89 μV/K at 623 K, which is approximately 50% less as compared to bare sample at room temperature. This result suggests that large size Ag particles for CZTS/1 wt% Ag composite sample might be present as large Ag grains decreases Seebeck coefficient [40]. Ito et al. [41] also reported that the Seebeck coefficient and electrical resistivity generally decreases with addition of metal particles. Seebeck coefficient according to Mott relation is

$$S = \frac{8}{3eh^2}\pi^2 k_{B^2} m^* T\left(\frac{\pi}{3n}\right)^{2/3} \quad (1)$$

where k_B, e, h and T are Boltzmann constant, electric charge of carrier, Planck constant and temperature respectively, m* is the effective mass and n is the charge carrier concentration [25]. Hence by combining the dependence on increased carrier concentrations or effective mass of carriers, overall Seebeck coefficient decreases with the addition of Ag NPs to CZTS matrix. But the degree of the S reduction with increase in Ag amount is moderate in contrast to the increase in electrical

Table 1
Comparison of thermoelectric properties of present work at 623 K with other's work of CZTS synthesized by different methods with additives/dopants[a].

Additive/Dopant	Method	σ (S/m)	S (μV/K)	κ (W/mK)	PF (μW/mK^2)	ZT	Ref.
–	Solution + SPS	30.94	889	1.17	24.8	0.013	[15]
–	Microwave + HP	1082	226	0.49	55.9	0.069	[This work]
–	Hydrothermal	5075	60	0.29	18.27	0.044	[17]
Cu	Hot injection + HP	1130	261	0.66	77.1	0.073	[15]
–	Solid state + SPS	~400	354	1.52	~40	0.021	[14]
Cu	Solid state + SPS	~11,100	190	1.14	~400	0.24	[14]
Ni	Colloidal + HP	2378	273	0.34	177.2	0.31	[16]
–	Colloidal + HP	632	240	0.67	36.4	0.030	[16]
–	Flow reactor	4717	128	–	77.2	–	[18]
Ag(0.5%)	Microwave + HP	4016	171	0.42	117.2	0.17	[This work]
Ag(1%)	(Microwave + HP	11,061	87	0.67	84.6	0.082	[This work]

[a] SPS: spark plasma sintering; HP: hot pressing.

conductivity.

Power factor (PF) values for all the composites are calculated by using σ and S in relation $PF = \sigma S^2$ and are shown in Fig. 8. (c). PF values for all the composites increase with the increasing temperature. Due to the increased electrical conductivity and slightly reduced Seebeck coefficient, highest power factor is observed for the CZTS/0.5 wt% Ag composite. PF value for this composite at room temperature is 61 μW/mK^2 and increases to a value 117 μW/mK^2 at 623 K whereas PF value for the bare sample is varying from 16 μW/mK^2 to 55 μW/mK^2 for this temperature range. CZTS/1 wt% Ag composite is also exhibiting higher values of PF 25 μW/mK^2 to 84.6 μW/mK^2 for the 300–623 K temperature range due to the highest conductivity for this sample. The PF value improves almost 2 times for CZTS/0.5 wt% Ag composite compared to the bare CZTS sample at 623 K. The obtained power factor values for Ag incorporated CZTS samples are even high as compared to those of reported values for some other CZTS systems as shown in Table 1.

3.2.2. Thermal transport properties

The thermal conductivity for all the samples are determined by using relation, $\kappa = \lambda * d * Cp$, where λ is thermal diffusivity, d is density and Cp is the specific heat, respectively. Fig. 9. (a) represents the temperature variation of thermal conductivity (κ) for CZTS/ x wt% Ag (x = 0, 0.5, 1) composites. Thermal conductivity has dependence on two major components, $\kappa = \kappa_e + \kappa_l$, where electronic thermal conductivity (κ_e) is due to the heat carried by electrons and lattice thermal conductivity (κ_l) is due to the heat conduction by phonons. It is clear from the results of thermal conductivity as shown in Fig. 9(a) that a small addition of Ag (0.5 wt%) can reduce the thermal conductivity of CZTS most probably due to the additional scattering of phonon from the finely dispersed Ag particles in the sample [24,27]. Hence a reduced thermal conductivity (0.59–0.41 W/mK) in the temperature range 300–623 K is observed for the CZTS/0.5 wt% Ag compared to parent CZTS sample (0.59 −0.50 W/m K). For the composite CZTS/0.5 wt% Ag, value of κ is even lower as compared to Cu doped bulk and nanocrystal CZTS systems as can be seen in Table 1. As observed from HRTEM and SEM analysis for composites, presence of multiscale grains, newly formed CZTS/Ag interfaces and increased grain boundaries can produce intense phonon scattering on larger length scales, significantly reducing the lattice thermal conductivity [23]. Inset of Fig. 9(a) shows the reduced lattice thermal conductivity for the CZTS/0.5 wt% Ag composite than the parent CZTS. Also, the complex structures of quaternary chalcogenides contribute in the reduction of thermal conductivity [42]. Incorporation of higher content of Ag resulted in the increase of thermal conductivity (0.643 W/mK at 623 K) for CZTS/1 wt % Ag composite, which may be due to the increased contribution from the electronic thermal conductivity and larger κ value of Ag metal [29,38]. It also indicates the presence of large sized Ag particles for CZTS/1 wt% Ag composite [40]. But the obtained values of thermal conductivity for all the composites are still less or comparable to some other reported CZTS systems in Table 1.

Combining the electric and thermal transport properties, figure of merit (ZT) has been determined for all the three samples and ZT value increases with the increase in temperature for all the three samples. The bar diagram of ZT, PF and k at 623 K temperature for all the specimens is shown in Fig. 9. (b). Out of the three samples, ZT for the CZTS/0.5 wt % Ag has a maximum value of 0.17 at 623 K. The maximum ZT obtained for this compound is due to the combination of higher power factor and reduced thermal conductivity which are shown in the bar diagram comparison of all the three samples. The ZT value for the other two compounds CZTS/1 wt% Ag and bare CZTS sample are 0.082 and 0.069 respectively. Hence, there is 2.5-fold increase in ZT value and 2-fold increase in power factor values for CZTS/0.5 wt% Ag compared to bare sample. High Ag metal concentrations either increase the thermal conductivity or reduce the Seebeck coefficient to greater extent, thus decreasing the overall performance of material [31]. All the thermoelectric results of the other CZTS systems along with the present ones at 623 K are summarized in the Table 1. Comparing these results with the reported results of CZTS, it can be observed that addition of appropriate amount of Ag NPs to CZTS system can effectively optimize the thermoelectric properties of this material by increasing the electrical conductivity and reducing thermal conductivity.

4. Conclusions

Thermoelectric CZTS/(0, 0.5, 1) wt% Ag composites were fabricated from powders by physical mixing followed by the hot pressing of all the samples. It was found that the Ag is mainly present as second phase and Ag particles are dispersed on the surface and in between the grain boundaries. With the addition of Ag content, the remarkable increase in the electrical conductivity is observed, while the Seebeck coefficient moderately decreases. Superior power factor (PF) value 117 μW/mK^2 at 623 K is obtained for the CZTS/0.5 wt% Ag composite. Moreover, for this composite the thermal conductivity is also reduced due to more grain boundary scattering of phonons by Ag NPs. The improved power factor and reduced thermal conductivity resulted in a maximum ZT value of 0.17 at 623 K for CZTS/0.5 wt% Ag which is almost 2.5 times higher than parent CZTS. Hence, by selecting the adequate quantity of Ag NPs along with a suitable synthesis technique improved thermoelectric properties of this CZTS system can be achieved.

Acknowledgement

This work is financially supported by the Department of Science and technology, Women Scientist Scheme (DST/WOS-A), Ministry of Science, Government of India under the project grant sanctioned to Sarita Devi Sharma for file no. SR/WOS-A/PM-44/2016(G). SN would like to acknowledge the GGSIPU, India for the FRGS grant under award letter no. GGSIPU/DRC/Ph.D/Adm./2017/503. We would like to thank The Chairman, Central Research Instruments Facility, Sri Satya Sai Institute of Higher Learning, India for providing the HRTEM characterization.

References

[1] A. Shakouri, Recent developments in semiconductor thermoelectric physics and materials, Annu. Rev. Mater. Res. 41 (2011) 399–431.
[2] H. Alam, S. Ramakrishna, A review on the enhancement of figure of merit from bulk to nano thermoelectric materials, Nano Energy 2 (2) (2013) 190–212.
[3] A.J. Minnich, M.S. Dresselhaus, Z.F. Ren, G. Chen, Bulk nanostructured thermoelectric materials: current research and future prospects, Energy Environ. Sci. 2 (2009) 466–479.
[4] O. Appel, T. Zilber, S. Kalabukhov, O. Beeri, Y. Gelbstein, Morphological effects on the thermoelectric properties of $Ti_{0.3}Zr_{0.35}Hf_{0.35}Ni_{1+\delta}Sn$ alloys following phase separation, , J. Mater. Chem. C 3 (2015) 11653–11659.
[5] O. Appel, M. Schwall, D. Mogilyansky, M. Kohne, B. Balke, Y. Gelbstein, Effects of microstructural evolution on the thermoelectric properties of spark plasma sintered $Ti_{0.3}Zr_{0.35}Hf_{0.35}NiSn$ half-heusler compound, J. Electron. Mater. 42 (7) (2013) 1340–1345.
[6] R. Amatya, R.J. Ram, Trend for thermoelectric materials and their earth abundance, J. Electron. Mater. 41 (6) (2012) 1011–1019.
[7] Y. Gelbstein, $Pb_{1-x}Sn_xTe$ alloys: application considerations, J. Electron. Mater. 40 (5) (2011) 533–536.
[8] R. Vizel, T. Bargig, O. Beeri, Y. Gelbstein, Bonding of Bi_2Te_3 based thermoelectric legs to metallic contacts using $Bi_{0.82}Sb_{0.18}$ alloy, J. Electron. Mater. 45 (3) (2016) 1296–1300.
[9] P. Qiu, X. Shi, L. Chen, Cu-based thermoelectric materials, Energy Storage Mater. 3 (2016) 85–97.
[10] Z.H. Ge, L.D. Zhao, D. Wu, X. Liu, B.P. Zhang, J.F. Li, J. He, Low-cost, abundant binary sulfides as promising thermoelectric materials, Mater. Today 19 (2016) 227–239.
[11] K. Suekuni, T. Takabatake, Research Update: Cu–S based synthetic minerals as efficient thermoelectric materials at medium temperatures, APL Mater. 4 (2016) 104503–104511.
[12] D. Chen, Y. Zhao, Y. Chen, B. Wang, Y. Wang, J. Zhou, Z. Liang, Hot-injection synthesis of Cu-Doped $Cu_2ZnSnSe_4$ nanocrystals to reach thermoelectric zT of 0.70 at 450 °C, ACS Appl. Mater. Interfaces 7 (44) (2015) 24403–24408.
[13] B. Wang, H. Xiang, T. Nakayama, J. Zhou, B. Li, Theoretical investigation on thermoelectric properties of Cu-based chalcopyrite compounds, Phys. Rev. B 95 (3) (2017) 035201.

[14] M.L. Liu, F.Q. Huang, L.D. Chen, I.W. Chen, A wide-band-gap *p*-type thermoelectric material based on quaternary chalcogenides of Cu_2ZnSnQ_4 (Q=S,Se), Appl. Phys. Lett. 94 (20) (2009) 202103.
[15] H. Yang, L.A. Jauregui, G. Zhang, Y.P. Chen, Y. Wu, Nontoxic and abundant copper zinc tin sulfide nanocrystals for potential high-temperature thermoelectric energy harvesting, Nano Lett. 12 (2012) 540–545.
[16] C. Xiao, K. Li, J. Zhang, W. Tong, Y. Liu, Z. Li, P. Huang, B. Pan, H. Su, Y. Xie, Magnetic ions in wide band gap semiconductor nanocrystals for optimized thermoelectric properties, Mater. Horiz. 1 (2014) 81–86.
[17] X. Zheng, Y. Liu, Y. Du, Y. Sun, J. Li, R. Zhang, Q. Li, P. Chen, G. Zhao, Y. Fang, N. Dai, P-type quaternary chalcogenides of $Cu_2ZnSn(S,Se)_4$ nanocrystals: large-scale synthesis, bandgap engineering and their thermoelectric performances, J. Alloy. Compd. 738 (2018) 484–490.
[18] A. Shavel, D. Cadavid, M. Ibanez, A. Carrete, A. Cabot, Continuous production of Cu_2ZnSnS_4 nanocrystals in a flow reactor, J. Am. Chem. Soc. 134 (2012) 1438–1441.
[19] A.M. Dehkordi, M. Zebarjadi, J. He, T.M. Tritt, Thermoelectric power factor: enhancement mechanisms and strategies for higher performance thermoelectric materials, Mater. Sci. Eng. R. Rep. 97 (2015) 1–22.
[20] M.Y. Kim, Y.H. Yeo, D.H. Park, T.S. Oh, Thermoelectric characteristics of the $(Bi,Sb)_2(Te,Se)_3$ nanocomposites processed with nanoparticle dispersion, Ceram. Int. 38 (2012) S529.
[21] S.V. Faleev, F. Leonard, Theory of enhancement of thermoelectric properties of materials with nanoinclusions, Phys. Rev. B 77 (2008) 214304.
[22] M. Zebarjadi, K. Esfarjani, A. Shakouri, J.H. Bahk, Z. Bian, G. Zeng, J. Bowers, H. Lu, J. Zide, A. Gossard, Effect of nanoparticle scattering on thermoelectric power factor, Appl. Phys. Lett. 94 (2009) 202105.
[23] Q. Zhang, X. Ai, L. Wang, Y. Chang, W. Luo, W. Jiang, L. Chen, Improved thermoelectric performance of silver nanoparticles-dispersed Bi_2Te_3 composites deriving from hierarchical two-phased heterostructure, Adv. Funct. Mater. 25 (2015) 966–976.
[24] Y. Lin, S. Sun, Q. Zhang, H. Shen, Q. Shao, L. Wang, W. Jiang, W. Jiang, Preparation of AgNPs/$Ca_3Co_4O_9$ nanocomposites with enhanced thermoelectric performance, Mater. Today Commun. 6 (2016) 44–49.
[25] K.H. Lee, H.S. Kim, S.I. Kim, E.S. Lee, S.M. Lee, J.S. Rhyee, J.Y. Jung, I.H. Kim, Y. Wang, K. Koumoto, Enhancement of thermoelectric figure of merit for $Bi_{0.5}Sb_{1.5}Te_3$ by metal nanoparticle decoration, J. Electron. Mater. 41 (6) (2012) 1165–1169.
[26] M. Ibanez, Z. Luo, A. Genc, L. Piveteau, S. Ortega, D. Cadavid, O. Dobrozhan, Y. Liu, M. Nachtegaal, M. Zebarjadi, J. Arbiol, M.V. Kovalenko, A. Cabot, High-performance thermoelectric nanocomposites from nanocrystal building blocks, Nat. Commun. 7 (2016) 10766.
[27] X. Zhou, G. Wang, L. Zhang, H. Chi, X. Su, J. Sakamoto, C. Uher, Enhanced thermoelectric properties of Ba-filled skutterudites by grain size reduction and Ag nanoparticle inclusion, J. Mater. Chem. 22 (2012) 2958–2964.
[28] G. Li, J. Yang, Y. Luo, Y. Xiao, L. Fu, M. Liu, J. Peng, Improvement of thermoelectric properties of In_4Se_3 bulk materials with Cu nanoinclusions, J. Am. Ceram. Soc. 96 (9) (2013) 2703–2705.
[29] S. Wang, Z. Bai, H. Wang, Q. Lu, J. Wang, G. Fu, High temperature thermoelectric properties of $Bi_2Sr_2Co_2O_y$/Ag composites, J. Alloy. Compd. 554 (2013) 254–257.
[30] L. Gao, S. Wang, R. Liu, X. Zha, N. Sun, S. Wang, J. Wang, G. Fu, Enhanced thermoelectric performance of CdO: Ag nanocomposites, Dalton Trans. 45 (30) (2016) 12215–12220.
[31] Y. Liu, D. Cadavid, M. Ibanez, S. Ortega, S.M. Sanchez, O. Dobrozhan, M.V. Kovalenko, J. Arbiol, A. Cabot, Thermoelectric properties of semiconductor-metal composites produced by particle blending, APL Mater. 4 (2016) 104813.
[32] B. Ananthoju, J. Mohapatra, M.K. Jangid, D. Bahadur, N.V. Medhekar, M. Aslam, Cation/anion substitution in $Cu_2ZnSnS_4$for improved photovoltaic performance, Sci. Rep. 6 (2016) 35369.
[33] Y. Lei, C. Cheng, Y. Li, R. Wan, M. Wang, Microwave synthesis and enhancement of thermoelectric figure of merit in half-Heusler $TiNiSb_xSn_{1-x}$, Ceram. Int. 43 (2017) 9343.
[34] S.D. Sharma, S. Neeleshwar, Thermoelectric properties of hot pressed CZTS micro spheres synthesized by microwave method, MRS Adv. 3 (24) (2018) 1373–1378.
[35] C.H. Ruan, C.C. Huang, Y.J. Lin, G.R. He, H.C. Chang, Y.H. Chen, Electrical properties of $Cu_xZn_ySnS_4$ films with different Cu/Zn ratios, Thin Solid Films 550 (2014) 525–529.
[36] C. Li, M. Cao, J. Huang, L.J. Wang, Y. Shen, Mechanism study of structure and morphology control of solvothermal synthesized Cu_2ZnSnS_4 nanoparticles by using different sulphur precursors, Mater. Sci. Semicon. Proc. 31 (2015) 287–294.
[37] S.A. Vanalakar, S.W. Shin, G.L. Agawane, M.P. Suryawanshi, K.V. Gurav, P.S. Patil, J.H. Kim, Effect of post-annealing atmosphere on the grain-size and surface morphological properties of pulsed laser deposited CZTS thin films, Ceram. Int. 40 (2014) 15097–15103.
[38] A. Nozariasbmarz, Z. Zamanipour, P. Norouzzadeh, J.S. Krasinski, D. Vashaee, Enhanced thermoelectric performance in metal/semiconductor nanocomposite of iron silicide/silicon germanium, RSC Adv. 6 (2016) 49643–49650.
[39] C. Zeng, S. Butt, Y.H. Lin, M. Li, C.W. Nan, Enhanced thermoelectric performance of $SmBaCuFeO_{5+d}$/Ag composite ceramics, J. Am. Ceram. Soc. 99 (2016) 1266–1270.
[40] C. Liu, L. Miao, J. Zhou, R. Huang, S. Tanemura, Bottom-up assembly to Ag nanoparticles embedded Nb-doped TiO_2 nanobulks with improved n-type thermoelectric properties, J. Mater. Chem. 22 (2012) 14180–14190.
[41] M. Ito, D. Furumoto, Effects of Ag addition on microstructure and thermoelectric properties of $Na_xCo_2O_4$ synthesized by citric acid complex process, Mater. Trans. 48 (2007) 3160–3163.
[42] Q. Chen, Y. Yan, H. Zhan, W. Yao, Y. Chen, J. Dai, X. Sun, X. Zhou, Enhanced thermoelectric performance of chalcogenide $Cu_2CdSnSe_4$ by ex-situ homogeneous nanoinclusions, J. Materiomics 2 (2016) 179–186.